ASTRONOMY & ASTROPHYSICS
SUPPLEMENT SERIES

Astron. Astrophys. Suppl. Ser. **120,** 89-98 (1996)

A 15 years monitoring program at 408 MHz*

M. Bondi[1], L. Padrielli[1], R. Fanti[1,2], A. Ficarra[1], L. Gregorini[1,2] and F. Mantovani[1]

[1] Istituto di Radioastronomia del CNR, Via Gobetti 101, I-40129, Bologna, Italy
[2] Dipartimento di Fisica, Università di Bologna, Via Irnerio 46, I-40126, Bologna, Italy

Received February 26; accepted April 9, 1996

Abstract. — This is the second paper based on the 408 MHz monitoring program with the East-West arm of the Bologna interferometer. The monitoring concerned 125 radio sources measured approximately once a month for 15 years. We present the summary of the variability analysis concerning all the sample and the monitoring data, not yet published, of the variable sources.

Key words: galaxies: active — quasars: general — radio continuum: galaxies

1. Introduction

This paper presents the results of a 15 years monitoring program at 408 MHz to investigate the low frequency variability of extragalactic radio sources.

The observations started in 1975 with an initial sample of 50 radio sources, known or suspected to be low frequency variable and known to be variable at frequencies higher than $\sim$ 1 GHz. In 1977 this sample was implemented by adding: a) 19 low frequency variable sources discovered by Cotton (1976a,b); b) a homogenous sample of 32 small angular diameter radio sources with diameter less than 1 arcsec, selected on the basis of scintillation studies (Cohen et al. 1967; Harris & Hardebeck 1969); c) a homogeneous sample of 45 flat spectrum radio sources ($\alpha < 0.5$ with $S \propto \nu^{-\alpha}$) taken from Veron et al. (1974). In 1982, 12 new objects (0106+319, 0235+164, 0300+47, 0336−019, 0415+37, 0528+134, 0727−11, 0814+42, 0851+202, 1308+32, 2121+05, and 2128+048), known to be extremely variable at higher frequencies (Aller, private communication), were added to the monitored sample. These 12 radio sources were observed only for 2.5 years. Finally, in 1984 2 radio sources at low galactic latitude (0622+14 and 0629+10) were included in the source list. The total number of monitored radio sources was 125, some sources being in common with different sub-samples.

The data till March 1979 were published in Fanti et al. (1981), hereafter referred as Paper I, and a multifrequency statistical analysis comprising light curves till 1983 was published in Padrielli et al. (1987). We present here the final summary of the 408 MHz monitoring program. All the data obtained in the period 1975-1990 are available in electronic form at the CDS via anonymous ftp at 130.79.128.5. These data, already been used in Spangler et al. (1993) and Bondi et al. (1994) for statistical analysis and interpretation of the refractive interstellar scintillation, could be useful to the astronomical community for multifrequency analyses.

2. Observations and data reduction

The 408 MHz observations were done using the East-West arm of the Northern Cross interferometer approximately once a month till the end of 1984. Each observation consisted of runs of 4-5 days, during which each source was often observed more than once. Starting from 1985 the observations became more erratic, usually organized in runs of 2-3 days every few months, and were also suspended from the end of 1985 till 1988. The monitoring program was definitively stopped in 1990.

The telescope output consists of three independent beams, 5 arcmin apart in hour angle. Each beam has an HPBW of $4' \times 100'$ arcmin.

The instrument stability was found to be better than 2% over a period of a few hours although it showed gain drifts of $\sim 2-6\%$ over time interval of several hours. Therefore, to determine the performances of the antenna, a sample of calibration sources, spread over the entire sky, were observed every one or two hours throughout each run. Most of the calibrators are 3C sources listed within the

Send offprint requests to: M. Bondi, Istituto di Radioastronomia, Via Gobetti 101, 40129 Bologna, Italy

*Tables 1 and 2 are also available in electronic form as LaTex files at the CDS via anonymous ftp 130.79.128.5, Tables 3-63 are only available in electronic form as ASCII files at the CDS via anonymous ftp 130.79.128.5

B2 catalogue and their flux densities were redetermined every 4-5 years as the average of the previous years flux density measurements. The internal consistency of the flux densities is believed to be better than 1%.

Since it is not our intention to measure absolute flux densities of the radio sources, we only discuss the errors affecting the internal consistency of the observations in order to detect radio variability.

In Table 1 we give the list of the calibration sources with the name of the source, an alias name, the average flux density ($\bar{S}$) in Jy, the rms scatter ($\sigma_{\rm rms}$) of the flux density measurements in Jy, and the number of observations (n). The data reduction has been performed in a way which is similar to that of Paper I, with particular care given to the noise evaluation and to the gain stability of the antenna.

Table 1. Calibrator sources

Name		$\bar{S}$	$\sigma_{\rm rms}$	n
0023−263	PKS	16.70	0.21	72
0123+329	3C 41	7.77	0.12	66
0133+206	3C 47	12.48	0.13	87
0316+413	3C 84	27.06	0.35	87
0345+337	3C 93.1	6.24	0.10	55
0433+295	3C 123	118.76	0.99	70
0450+314	3C 131	8.98	0.11	77
0459+252	3C 133	13.57	0.21	43
0501+380	3C 134	34.88	0.26	88
0523+327	3C 141	7.34	0.12	39
0640+233	3C 165	7.00	0.07	76
0710+118	3C 175	8.63	0.11	87
0802+243	3C 192	10.93	0.13	88
0915−118	HYD.A	129.92	1.91	72
1006+077	3C 237	15.76	0.23	72
1142+318	3C 265	9.76	0.11	89
1151+295	4C 29.44	4.94	0.09	82
1251+278	3C 277.3	6.64	0.09	67
1350+316	3C 293	9.74	0.11	82
1409+524	3C 295	50.89	0.60	86
1514+072	3C 317	25.56	0.51	63
1626+396	3C 338	17.67	0.16	93
1828+487	3C 380	34.31	0.48	77
1842+455	3C 388	14.63	0.12	80
2018+295	3C 410	23.15	0.22	77
2121+248	3C 433	32.86	0.39	79
2314+038	3C 459	15.04	0.19	92
2348+643	3C 468.1	18.82	0.26	65

The sample of observed calibrators, uniformly spread over the entire set of declinations and sideral time, allows the determination for each run of:

1. the trend of the antenna gains as a function of time; this is generally known with a 2% accuracy.
2. the variation of the antenna gain with declination, which may differ from one run to another.

After the flux densities of the radio sources have been corrected for the variations of the instrumental gain, which depend on time and declination, it is possible to correctly evaluate the residual percentage error due to calibration ($\sigma_{\%}$). At the same time, it is possible to estimate the noise error in each run ($\sigma_{\rm n}$), by direct comparison of the flux densities measured by three indipendent beams. In such a way, the flux error associated with each source of flux density S can be defined as follows:

$$\sigma_\epsilon = \sqrt{\sigma_{\rm n}^2 + \sigma_{\%}^2 S^2} \qquad (1)$$

This error could be different from run to run and is a reliable indicator of the quality of the observations. The distribution of $\sigma_{\rm n}$ and $\sigma_{\%}$ are shown in Fig. 1. The median values are 0.07 Jy and 1.4% respectively .

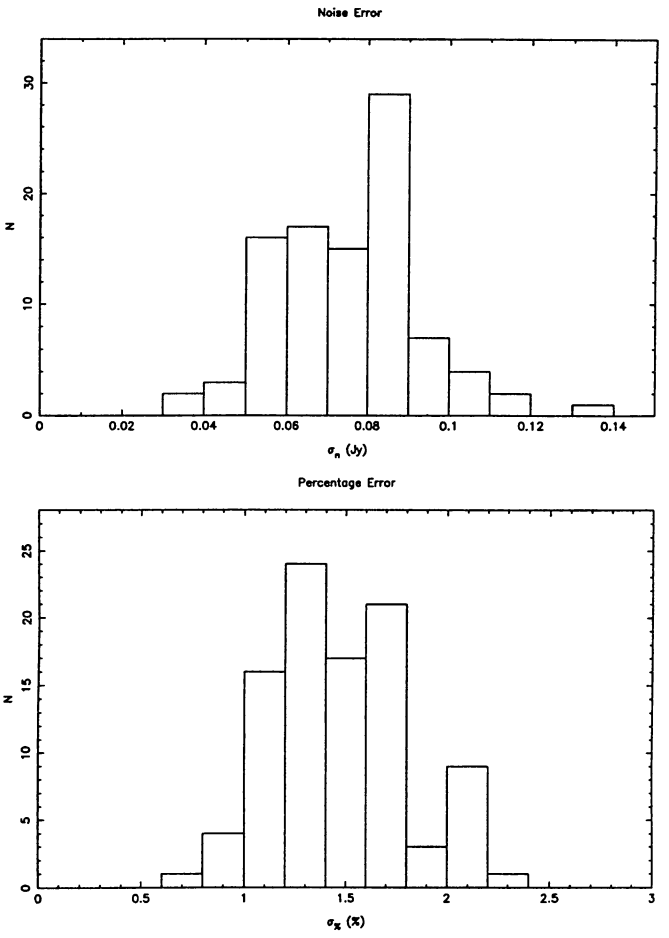

Fig. 1. Distribution of the noise error ($\sigma_{\rm n}$) and the percentage error ($\sigma_{\%}$) over all the observing runs

The random changes of the dependence of the instrumental gain with the declination depend on the mechanical distorsions of the mirror, different from period to period.

Particular care was spent in the analysis of the interplanetary scintillation, which may cause flux density

fluctuations as large as 100% when the line of sight to a radio source is close to the Sun. When the observed radio source was not far from the Sun and its flux density was affected by interplanetary scintillation, the percentage error applied to the flux measurements has been defined as proportional to the measured scintillation percentage (which is an upper limit for the error estimate), i.e.:

$$\sigma_{\%} = \frac{\Delta S_{\rm scin}}{2S\sqrt{N}} \tag{2}$$

where N is the number of source measurements in the run, $\Delta S_{\rm scin}$ the maximum flux density variation, and S the average flux density measured in the run. In any case, to all the sources within 30° from the Sun, we attributed a percentage error never lower than 5%, even if no flux density fluctuations were evident.

These lower quality measurements have not been used in the variability analysis. For sources at an angular distance larger than 30° to the Sun, the flux density fluctuation due to scintillation has been estimated to be generally smaller than 5% on each beam and its effect on the flux density, averaged over several measures, is less than the calibration errors.

3. Results

After the set of flux densities and their errors have been obtained for each epoch, the weighted average flux for each source has been calculated using the relation:

$$\bar{S} = \frac{\sum_{i=1}^{n} S_i/(\sigma_\epsilon^2)_i}{\sum_{i=1}^{n} 1/(\sigma_\epsilon^2)_i} \tag{3}$$

Where S_i and $(\sigma_\epsilon)_i$ are the measured flux density and estimated error for the i-th epoch, and n is the number of valid measurements.

Following the statistical analysis used in Paper I, we then calculated the chi-squared:

$$\chi^2 = \sum_{i=1}^{n} \frac{(S_i - \bar{S})^2}{(\sigma_\epsilon^2)_i} \tag{4}$$

We considered variable the sources with a probability that the flux density variations were due to random changes $p(\chi^2) < 0.1\%$ and possibly variable those with $2\% > p(\chi^2) > 0.1\%$.

We did not include in either group those sources whose large χ^2 value was mainly due to one single measure not confirmed by further measurements during the same run. This procedure prevents interpreting as variability fortuitous bad results, but might cause the loss of short outbursts. The magnitude of the variability can be characterized by the rms scatter of the flux densities deconvolved by the estimated error:

$$\sigma_{\rm var} = \sqrt{\sigma_{\rm rms}^2 - \sigma_\epsilon^2} \tag{5}$$

Figure 2 shows the distribution of the reduced χ_n^2 ($\chi_n^2 = \chi^2/(n-1)$) for all the sources: the filled area of the histogram include the variable sources and the hatched area the probable variable sources.

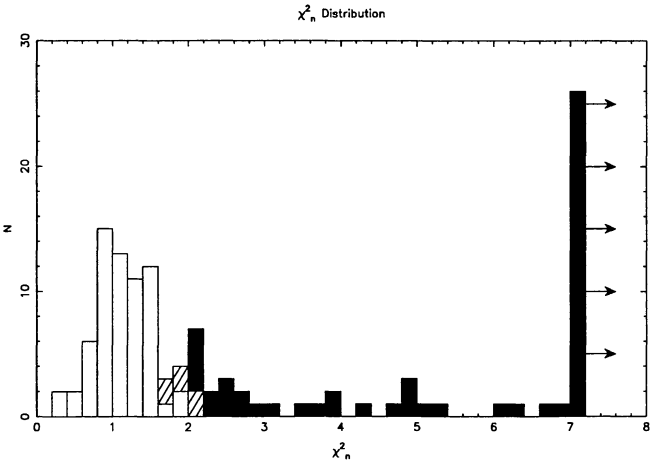

Fig. 2. Distribution of the χ_n^2: filled area shows variable sources and hatched area indicates probable variable sources

In Table 2 we give the essential information for each source: names, optical identification, redshift, average flux density at 408 MHz in Jy, $\sigma_{\rm var}$ in Jy only for the variable and probable variable sources, and χ_n^2. The last four columns of Table 2 list the number of valid measures, the first and last epoch of observation (yr −1900) and a code identifying the variable (V) and probably variable (P) radio sources.

The χ^2 analysis is powerful in detecting those radio sources whose measurements give an rms larger than that statistically expected, but it does not tell us anything about the timescale of the variability and its temporal characteristics. A full analysis of the timescales of the variable radio sources was published in Bondi et al. (1994).

Among the 125 radio sources of the monitoring program, 55 are found to be variable and 6 probable variable. All the sources found variable in Paper I after 5 years of monitoring remain classified as variable, while two sources, previously classified as P in Paper I, are found not variable after a longer monitoring and increased statistics. In spite of the relatively short monitoring interval (2.3 years), 10 out of the 12 sources with strong variability at higher frequency are found to be variable. This confirms that radio sources strongly variable at high frequency are the best candidates for detection of low frequency variability regardless of which mechanism is responsible for the low frequency variability.

The radio sources 0622+14 (galactic coordinates l = 197° and b = 1°) and 0629+10 (galactic coordinates l = 202° and b = 0.5°), added to the monitored list in 1984, are found to be not variable. Ghosh & Rao (1992) do not detect any significant variability in 0629+10 at

Table 2. Summary of monitored sources

Name		Id	z	$\bar{S}$	$\sigma_{\rm var}$	χ^2_n	n	First	Last	Code
0003−003	3C 2	Q	1.04	9.51		0.98	27	75.5	84.7	
0019−000	DA 009	G		2.93		1.85	13	77.4	80.1	
0034−014	3C 15	G	0.07	10.35		0.98	40	75.5	84.7	
0051+317	B2			1.75		1.51	21	76.8	82.5	
0056−001	DA032	Q	0.72	3.98	0.10	2.24	44	77.4	84.7	V
0106+013		Q	2.10	2.95	0.07	1.95	20	82.4	84.7	P
0107+563	4C56.02	Q		4.30		1.08	36	77.5	82.8	
0116+319	B2	G		3.51		0.95	33	77.5	84.7	
0116+082	4C08.06	G	0.59	4.96		1.11	16	77.4	82.9	
0127+233	3C 43	Q	1.46	6.90		0.61	44	75.5	84.7	
0128+039	OC+047			5.10		0.97	12	77.5	80.1	
0134+329	3C 48	Q	0.37	36.63		0.72	27	75.5	83.9	
0138+136	3C 49	G	0.62	6.77		0.74	17	77.3	84.7	
0202+149	NRAO91	Q		5.61	0.21	5.29	50	77.4	90.2	V
0221+276	3C 67	G	0.31	7.45		1.26	19	77.3	85.2	
0223+341	4C34.07			3.63		1.52	17	77.5	82.9	
0224+671	4C67.05	Q		3.95	0.21	8.16	85	75.6	90.2	V
0235+164		BL		1.68	0.11	3.59	19	82.4	84.7	V
0240−002	3C 71	G	0.004	11.34		0.67	40	75.5	83.7	
0251+200	NRAO117			3.80		1.14	44	76.7	84.7	
0300+47	4C47.08	BL		1.71	0.14	6.23	21	82.4	84.7	V
0316+413	3C 84	G	0.02	27.06		0.97	73	75.5	90.2	
0316+162	CTA 21	Q		8.06		1.49	48	75.5	84.7	
0320+053	DA10 1	G		6.49	0.21	3.93	38	77.5	84.7	V
0333+321	NRAO140	Q	1.26	2.93	0.31	21.70	70	75.5	90.2	V
0336−019		Q	0.85	2.00	0.40	35.94	19	82.4	84.7	V
0345+337	3C93.1	G	0.24	6.24		0.94	45	77.3	90.2	
0348+175	PKS	G		3.23	0.07	1.72	62	76.8	84.7	P
0355+508	NRAO150	Q		6.66		1.34	43	75.5	82.9	
0358+004	3C 99	G	0.43	4.97	0.11	2.09	63	77.7	90.2	V
0402+160	NRAO161			2.17	0.06	1.64	46	77.2	84.7	P
0405−123	KS	Q	0.57	8.05		1.16	46	75.5	82.1	
0411+101	3C109	G	0.31	11.84		0.81	61	75.5	84.0	
0415+37				28.70		0.57	23	82.4	84.7	
0422+178				1.90	0.11	2.92	19	76.8	83.2	V
0422+005	OF038	BL	0.31	1.35	0.06	1.91	69	75.5	84.7	P
0428+205	PKS	G	0.22	2.82		0.85	12	77.5	80.2	
0430+052	3C120	G	0.03	5.72	0.56	25.47	70	75.5	90.2	V
0518+165	3C138	Q	0.76	16.61	0.23	2.38	47	77.5	90.2	V
0528+134		Q	2.06	1.19	0.06	2.15	21	82.4	84.7	P
0538+498	3C147	Q	0.55	46.78		1.12	33	77.5	84.7	

327 MHz. Moreover they find that the scintillation index shows a dependence on galactic latitude peaking around $|b| \sim 15°$ and decreasing at low and high latitudes. This can be explained if the line of sight to the source crosses a region of very large scattering (e.g. the galactic centre). In this case, the timescale for refractive interstellar scintillation could be much longer than the observing interval of the monitoring (Spangler et al. 1989). Alternatively, it is possible that the simplified geometrical model used to characterize the distribution of the scattering in the Galaxy (higher scattering at low galactic latitudes and in the direction of the Galactic centre, lower scattering at increasing galactic latitudes) is not adequate. Ghosh & Rao (1992) using a distribution of the scattering material that follows the spiral arms of the Galaxy find a minimum in the predicted scintillation indeces for $|b| < 5°$.

In Fig. 3 we show a few light curves which can be considered as typical of the different variability behaviours. In many cases, the flux density variations seem to occur smoothly with typical time intervals between relative minimum and maximum of about one or two years (e.g. 0333+321, 0736+017, 1611+343, and 2251+151 in Fig. 3). Some sources show a more rapid variability with timescales of the order of a few months (e.g. 0336−019,

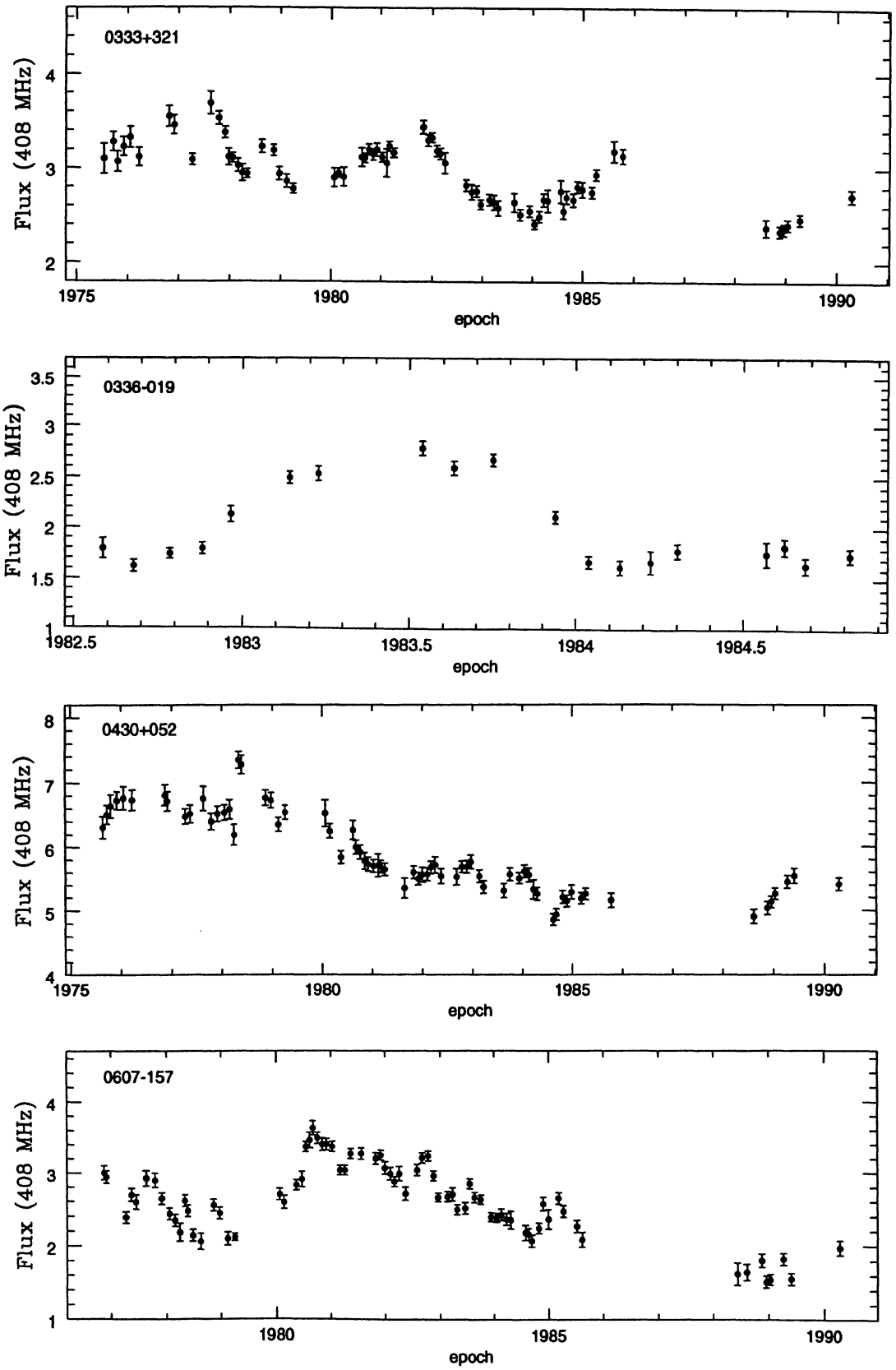

Fig. 3. Light curves at 408 MHz of 0333+321, 0336−019, 0430+052, 0607−157, 0736+017, 0859−140, 1117+146, 1611+343, 1633+382, 1641+399, 2200+420, and 2251+151

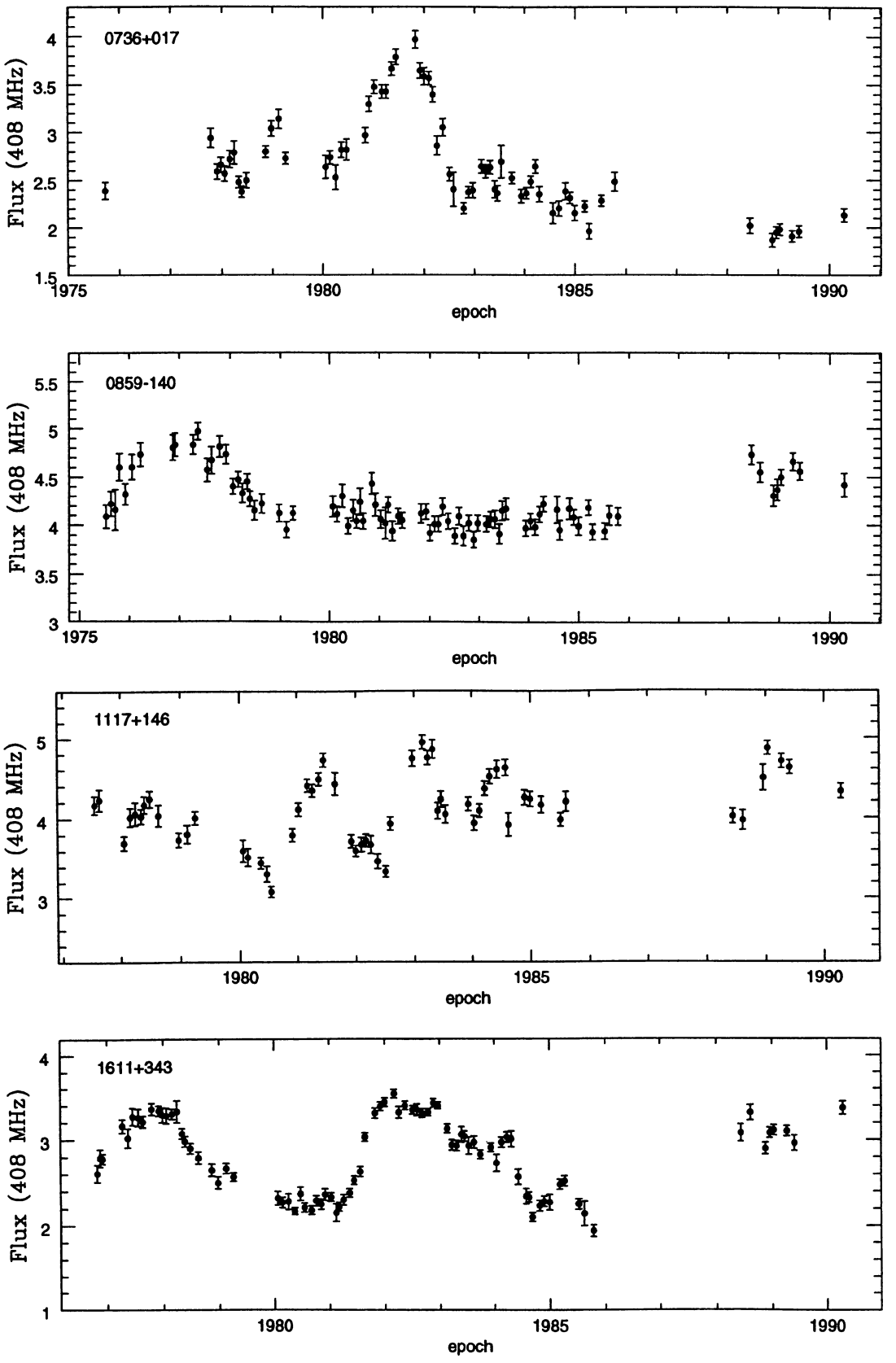

Fig. 3. continued

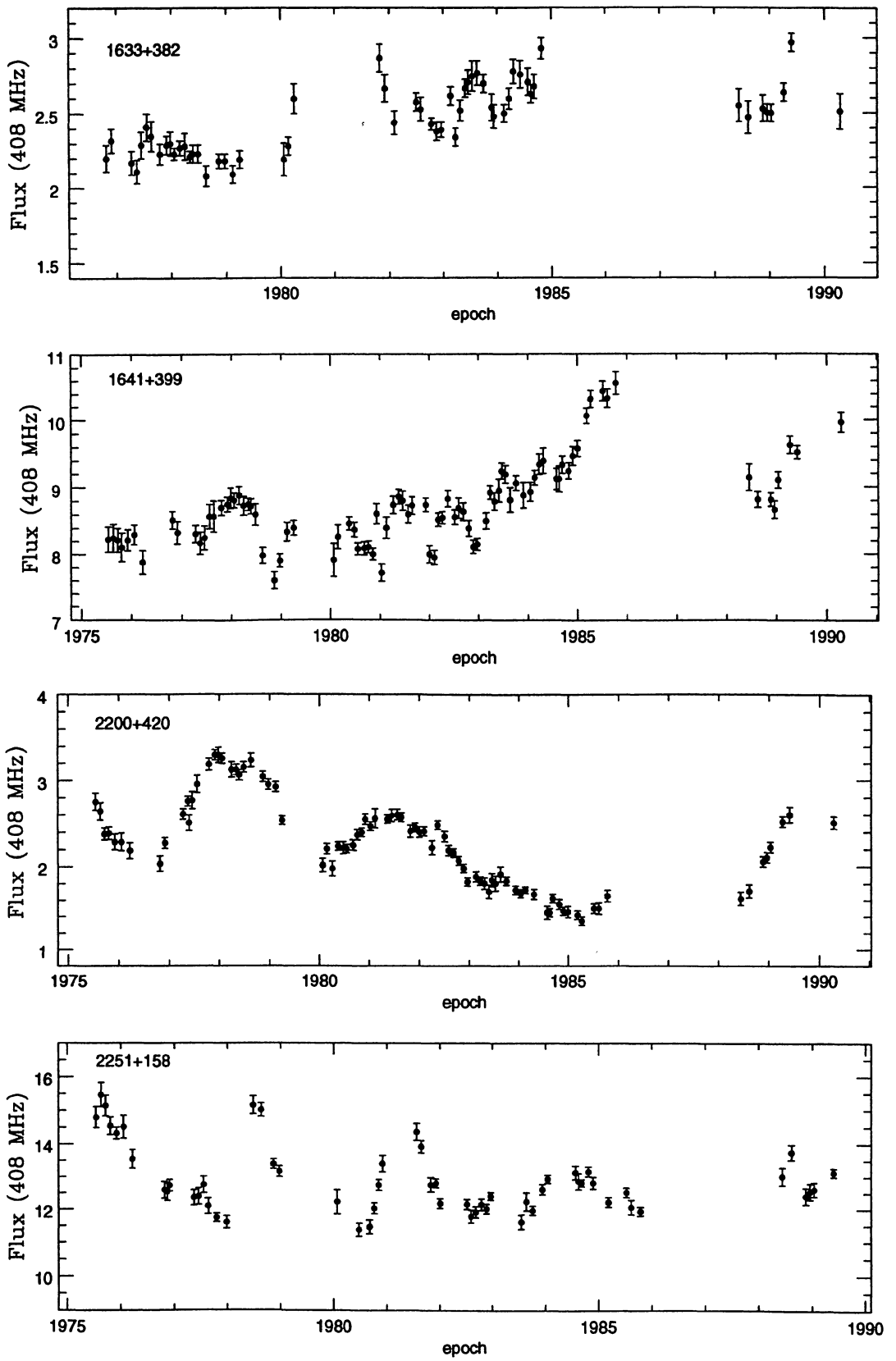

Fig. 3. continued

Table 2. continued

Name		Id	z	$\bar{S}$	$\sigma_{\rm var}$	χ^2_n	n	First	Last	Code
0548+165	DA190	Q		4.17	0.17	6.15	57	77.4	90.2	V
0603+203	3C152			6.76		0.90	13	77.6	80.1	
0605−085	PKS	Q	0.87	3.83	0.34	15.08	73	75.6	90.2	V
0607−157	PKS	Q	0.32	2.63	0.48	37.38	76	76.8	90.2	V
0618+145	3C158			7.88		0.33	55	76.7	84.7	
0621+400	3C159	G	0.48	6.39	0.17	3.16	76	75.5	89.3	V
0622+14				5.61		0.76	12	84.8	90.2	
0629+10				2.52		1.08	13	84.8	90.2	
0631+191				2.68	0.08	2.65	63	76.8	84.7	V
0659+445	4C44.15			6.84		1.31	14	77.5	84.5	
0723−008	DW	G	0.13	3.32	0.20	7.66	60	75.6	84.7	V
0727−11				2.12		1.27	22	82.4	84.7	
0735+178	PKS	BL	0.42	1.99	0.13	3.85	28	75.8	82.9	V
0736+017	OI+161	Q	0.19	2.60	0.50	46.34	66	75.6	90.2	V
0738+313	OI+363	Q	0.63	1.59	0.07	2.02	54	76.0	84.7	V
0812+488	3C196	Q	0.87	38.14		1.52	29	78.2	82.5	
0814+42				1.68	0.24	17.63	20	82.4	84.7	V
0831+557	4C55.16	G	0.24	8.48		0.99	11	77.5	80.1	
0834−20	PKS	Q	2.74	3.41	0.16	4.94	67	75.7	84.7	V
0851+202		B	0.31	1.32	0.12	4.72	18	82.4	84.7	V
0855+280	3C210	G	1.17	5.85		1.06	15	77.4	80.1	
0859−140	OJ−199	Q	1.34	4.19	0.24	7.66	83	75.5	90.2	V
0923+392	4C39.25	Q	0.70	3.50		1.59	57	75.5	82.9	
0933+045	3C222	G		5.27		0.94	40	77.5	84.7	
0945+408	4C20.24	Q	1.11	2.70	0.11	3.66	56	77.4	84.7	V
0958+255	4C25.30			1.49		0.50	47	76.8	82.9	
1006+077	3C237	G	0.88	15.76		0.80	59	75.5	90.2	
1019+222	3C241	G	1.62	6.46		1.10	54	76.7	84.7	
1055+018	4C01.28	Q	0.89	4.13	0.16	4.20	74	75.5	90.2	V
1101+384	B2	G	0.03	1.16		1.03	21	76.0	80.1	
1116+128	4C12.39	Q	2.12	3.61		1.52	58	75.5	84.6	
1117+146	PKS	Q	1.20	4.06	0.44	23.02	59	77.5	90.2	V
1118+237	3C256	G	1.82	4.90		1.77	14	77.5	80.1	
1123+303	4C30.11	G		2.93		0.34	27	76.8	82.9	
1127−145	OM−146	Q	1.19	5.53	0.30	7.85	71	75.5	90.2	V
1148−001	PKS	Q	1.98	3.35	0.09	2.00	50	77.5	84.6	V
1151+295	4C29.44	G	0.33	4.94		0.94	82	75.6	90.2	
1156+295	4C29.45	Q	0.73	2.74	0.14	4.89	76	75.6	90.2	V
1226+023	3C273	Q	0.16	60.16		1.54	66	75.5	84.7	
1253−055	3C279	Q	0.5	13.79	0.65	8.39	67	75.6	90.2	V
1308+32		BL	1.00	1.40	0.07	2.72	24	82.4	84.7	V
1328+307	3C286	Q	0.85	23.51		0.80	50	75.5	85.4	
1328+254	3C287	Q	1.06	13.09		1.28	33	75.5	84.5	
1345+125	4C12.50	G	0.12	7.90		1.00	17	77.5	82.0	
1358+624	4C66.22	G	0.43	5.76	0.24	7.50	69	77.5	90.2	V

and 1117+146 in Fig. 3), while others display drifts in the light curves indicative of timescales of many years (e.g. 0430+052, and 2200+420 in Fig. 3). Short and long timescales can be both present on the same source (e.g. 0607−157, and 1641+399 in Fig. 3). Finally some sources display prolonged period of inactivity (e.g. 0859−140, and 1633+382 in Fig. 3).

In Tables 3-63 (only available in electronic form at the CDS via anonymous ftp at 130.79.128.5), all the observational data for each individual variable or possibly variable object are given. For each source, we list the epoch of observations, the number of times the source was observed in each run (between 1 and 4), the flux density and the associated estimated error in Jy, the percentage of scintillation, and a code (−) identifying a measurement

Table 2. continued

Name		Id	z	$\bar{S}$	$\sigma_{\rm var}$	χ^2_n	n	First	Last	Code
1416+066	3C298	Q	1.44	24.44		1.38	38	75.5	84.5	
1422+202	4C20.33	Q	0.87	5.03	0.09	2.13	84	76.8	90.2	V
1454−060	PKS	Q	1.25	2.87		1.49	27	75.5	80.2	
1504−166	OR−102	Q	0.88	2.62	0.26	13.22	73	75.5	90.2	V
1510−089	OR−017	Q	0.36	2.81	0.25	11.18	70	75.5	90.2	V
1518+046	4C04.51	G		3.76		1.11	30	77.5	82.5	
1523+033	4C03.33			4.03		1.25	25	77.5	83.6	
1524−136	OR−140	Q	1.69	5.59	0.46	18.47	66	75.5	90.2	V
1611+343	DA 406	Q	1.40	2.81	0.45	54.48	85	76.7	90.2	V
1633+382	4C38.41	Q	1.81	2.43	0.21	11.21	59	76.7	90.2	V
1641+399	3C345	Q	0.60	8.70	0.57	21.17	88	75.5	90.2	V
1643−223	MSH			5.90		1.39	20	75.6	80.1	
1645+174	NRAO517	G	0.31	3.67	0.09	2.00	49	77.5	84.7	P
1726+318	3C357	G	0.17	5.92		0.86	35	77.4	82.2	
1729+211	4C21.50			1.88		1.16	24	76.8	82.9	
1730−130	NRAO530	Q	0.90	7.30	0.39	9.58	60	75.6	90.2	V
1828+487	3C380	Q	0.69	34.31		1.46	76	75.6	90.2	
1835+134	4C13.67			3.42		1.23	16	77.5	80.1	
1901+319	3C395	Q	0.64	4.98	0.26	12.65	68	77.4	90.2	V
2012+234	3C409			44.87		0.76	50	75.7	84.7	
2015+131	4C13.76			1.73		1.39	40	76.8	82.6	
2033+187	OW155.5			3.44	0.18	7.92	77	76.7	90.2	V
2056+445	4C44.37			2.15	0.06	2.17	44	77.2	84.7	V
2121+05		Q	1.88	1.33		6.70	22	82.4	84.7	V
2128+048	OX+046	G		3.67		1.08	13	77.5	80.1	
2131−02		BL	0.56	2.15		4.87	18	82.5	84.7	V
2134+004	DA553	Q	1.94	1.29	0.07	2.48	65	76.0	84.7	V
2145+067	DA562	Q	0.99	3.45	0.17	5.16	53	75.6	90.2	V
2147+145	PKS			6.57	0.16	2.53	27	77.2	90.2	V
2200+420	BL LAC	BL	0.07	2.24	0.50	7.76	86	75.5	90.2	V
2210+016	4C01.69			4.24		1.89	12	77.5	82.9	
2223−052	3C446	BL	1.40	11.83		1.31	50	75.6	84.7	
2223+210	DA580	Q	1.95	3.50	0.09	2.50	34	77.5	82.3	V
2230+114	CTA102	Q	1.04	7.71	0.33	6.97	61	75.5	90.2	V
2249+185	3C454	Q	1.76	5.53		1.45	19	76.0	83.2	
2251+158	3C454.3	Q	0.86	12.67	0.81	20.07	58	75.5	90.2	V
2255+415	4C41.45			3.79	0.23	8.25	63	77.5	90.2	V
2338+132	4C13.88			6.16		1.47	34	76.7	84.7	
2344+092	4C09.44	G		2.96		1.50	16	77.4	81.7	

affected by interplanetary scintillation and not used in the χ^2 analysis.

4. Summary of the results discussed in previous papers

In this section we summarize the results obtained in various papers using the 408 MHz monitoring data.

Data prior to 1984 were used in a multifrequency analysis spanning a frequency range of 0.4−14.5 GHz (Padrielli et al. 1987). Three distinct classes of variability were identified. The first class includes sources showing variability only at low frequency ($\nu \lesssim 1$ GHz). The second class contains sources which have both high and low frequency variability which appear unrelated, and have a minimum of activity around 1 GHz. The third class accounts for objects which show correlated variability from high to low frequency. These different characteristics are the signature of two distinct phenomena responsible for the variability. The high frequency variability and the correlated low frequency variability can be explained with the classical expanding synchrotron cloud model, possibly with relativistic bulk motions. The remaining sources show only low frequency variability, or uncorrelated high and low frequency variability. For these sources the low frequency variability might be explained as refractive interstellar scintillation.

Theoretical models of refractive interstellar scintillation were compared with the characteristics of the

low frequency variability as derived from the 408 MHz monitoring in a series of papers (Spangler et al. 1989; Mantovani et al. 1990; Spangler et al. 1993; Bondi et al. 1994). The main results of these investigations were the following.

1. In most of the cases where information on the milliarcsecond structure at low frequency are avalaible, the variability indices are consistent with those expected from a "standard model" for interstellar turbulence, i.e. turbulence with a Kolmogorov spatial power spectrum and galactic distribution as indicated by pulsar observations.
2. For a few sources, the scintillation indices are considerably greater than expected. It is possible that these large amplitude variations are caused by the same type of irregularities which produce occasional refractive phenomena in pulsar scintillations, such as interference pattern in dynamic spectra.
3. The agreement between observed and predicted variability timescales is generally poor, although there are a number of factors which plausibly could be responsible for this poor correlation.
4. A one-year modulation is found. This modulation is produced by the earth orbital motion through the scintillation pattern. A significant constrain on the propagation velocity of the interstellar turbulent irregularities is obtained ($V_{\rm irr} \lesssim 10$ km s^{-1}), suggesting that he motion between the Earth and the scattering pattern is, on average, mainly determined by the motion of the Earth-Sun system with respect to the Local Standard of rest and the Earth orbital motion around the Sun.

Finally, the Doppler factors derived from multi-epoch 18 cm VLBI observations were compared with those calculated from the 408 MHz variability over the same interval (Padrielli et al. 1986; Bondi et al. 1996). This comparison showed that for the majority of sources there is no correspondence between structural variations on the milliarcsecond scale and low frequency outbursts. In a minority of events, 408 MHz flux density variations and 18 cm VLBI structural variations are clearly related. These results reinforce the hypothesis that the low frequency variability in extragalactic radio sources is mainly due to an extrinsic mechanism affecting all compact (≤ 10 mas at 408 MHz) radio sources. As might be expected, the very compact intrinsic variables also show evidence for an extrinsic origin for some outbursts.

References

Bondi M., Padrielli L., Gregorini L., Mantovani F., Shapirovskaya N., Spangler S.R., 1994 A&A 287, 390
Bondi M., Padrielli L., Fanti R., et al., 1996, A&A, (in press)
Cohen M.H., Gunderman E.J., Harris D.E., 1967, ApJ 150, 767
Cotton W.D., 1976a, ApJ 204, L63
Cotton W.D., 1976b, ApJS 32, 467
Fanti C., Fanti R., Ficarra A., et al., 1981, A&AS 45, 61 (Paper I)
Ghosh T., Rao A.P., 1992, A&A 264, 203
Harris D.E., Hardebeck E.J.G., 1969, ApJS 19, 115
Mantovani F., Fanti R., Gregorini L., Spangler S.R., 1990, A&A 233, 535
Padrielli L., Aller M.F., Aller H.D., et al., 1987, A&AS 67, 63
Padrielli L., Romney J.D., Bartel N., et al., 1986, A&A 165, 53
Spangler S.R., Fanti R., Gregorini L., Padrielli L., 1989, A&A 209, 315
Spangler S.R., Eastman W.A., Gregorini L., Mantovani F., Padrielli L., 1993, A&A 267 213
Veron M.P., Veron P., Witzel A., 1974, A&AS 13, 1